Journal of Medicinal Chemistry

This article is made available via the ACS COVID-19 subset for unrestricted RESEARCH re-use and analyses in any form or by any means with acknowledgement of the original source. These permissions are granted for the duration of the World Health Organization (WHO) declaration of COVID-19 as a global pandemic.

pubs.acs.org/jmc

Article

Design and Evaluation of a Novel Peptide−Drug Conjugate Covalently Targeting SARS-CoV-2 Papain-like Protease

Na Liu,[#] Yichi Zhang,[#] Yingshou Lei,[#] Rui Wang, Meimiao Zhan, Jianbo Liu, Yuhao An, Yaoqi Zhou, Jian Zhan,* Feng Yin,* and Zigang Li*

Cite This: J. Med. Chem. 2022, 65, 876−884

Read Online

ACCESS | Metrics & More | Article Recommendations | Supporting Information

ABSTRACT: Coronavirus disease 2019 (COVID-19) pandemic, a global health threat, was caused by severe acute respiratory syndrome coronavirus 2 (SARS-CoV-2). The SARS-CoV-2 papain-like cysteine protease (PLpro) was recognized as a promising drug target because of multiple functions in virus maturation and antiviral immune responses. Inhibitor GRL0617 occupied the interferon-stimulated gene 15 (ISG15) C-terminus-binding pocket and showed an effective antiviral inhibition. Here, we described a novel peptide−drug conjugate (PDC), in which GRL0617 was linked to a sulfonium-tethered peptide derived from PLpro-specific substrate LRGG. The EM-C and EC-M PDCs showed a promising *in vitro* IC50 of 7.40 ± 0.37 and 8.63 ± 0.55 μM, respectively. EC-M could covalently label PLpro active site C111 and display anti-ISGylation activities in cellular assays. The results represent the first attempt to design PDCs composed of stabilized peptide inhibitors and GRL0617 to inhibit PLpro. These novel PDCs provide promising opportunities for antiviral drug design.

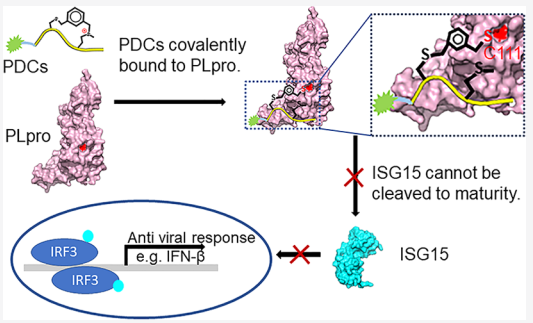

INTRODUCTION

Coronavirus disease 2019 (COVID-19) is a pandemic acute respiratory disease caused by severe acute respiratory syndrome coronavirus 2 (SARS-CoV-2), which threatens human health and public safety.[1,2] COVID-19 generally has a lower mortality rate than SARS but its infection rate, the number of infected people, and the spatial range of epidemic areas far exceed the SARS and the Middle East respiratory syndrome (MERS).[3] As of November 2021, the COVID-19 pandemic has resulted in more than 250 million confirmed cases and more than 5 million confirmed deaths according to the epidemiological updates of the World Health Organization (WHO).[4] In the past two years or so, the COVID-19 has caused devastating damage to the world.

Scientists have been working in the quest for possible preventive and therapeutic methods.[5−7] It is reported that eight vaccines were approved for full use for the first time, while the other six vaccines got approval for limited use against COVID-19.[7−9] However, the emergence of SARS-CoV-2 variants led to increased transmission and resistance, which is associated with antibody escape from the virus spike epitopes.[10] Currently, there is only one specific oral antiviral agent against SARS-CoV-2, namely, molnupiravir. Molnupiravir has a good safety profile, tolerability, and oral bioavailability in humans.[11,12] However, there are inherent risks in this approach such as molnupiravir-induced tumorigenesis and the emergence of detrimental mutations in sperm precursor cell generation and embryo development.[13] According to WHO global solidarity clinical trials, remdesivir, hydroxychloroquine, lopinavir, and interferon regimens that have completed clinical trials had little or no effect on hospitalized patients with COVID-19.[9,14] Therefore, current studies are focused on the rapid development of antiviral drugs to treat SARS-CoV-2 infection.

The papain-like protease (PLpro) is an attractive target in the antiviral drug design of SARS-CoV-2 and other coronaviruses (SARS, MERS, etc.) because of its multiple major functions.[15−19] PLpro is an essential coronavirus cysteine protease processing viral polyproteins to yield product nsp1, nsp2, and nsp3.[20] These products generated a functional replicase complex to initiate the replication and transcription of the viral genome.[20,21] The cleavage specificity of PLpro corresponds to the LXGG motif.[16,22] PLpro is also responsible for cleavage proteinaceous post-translational modifications on host proteins (deubiquitinating and deISGylating activities) as an evasion mechanism against host antiviral innate immune responses.[16,22−27] SARS-CoV-2 PLpro preferentially cleaves interferon-stimulated gene 15 (ISG15) to attenuate type-I interferon responses.[16] SARS-CoV PLpro is involved in inhibiting the production of cytokines and chemokines that

Received: November 24, 2021
Published: January 4, 2022

ACS Publications

© 2022 American Chemical Society

https://doi.org/10.1021/acs.jmedchem.1c02022
J. Med. Chem. 2022, 65, 876−884

are responsible for the activation of the host innate immune response against viral infection.[23,24,28]

Many scientists identified PLpro inhibitors in different approaches, such as virtual screening using small-molecule libraries such as Asinex library and FDA-approved inhibitor library.[14,29−31] Several compounds were identified as potential inhibitors of PLpro such as VIR250, VIR251, tanshinone IIA sulfonate sodium, and chloroxine.[17,31] In addition, noncovalent small-molecule SARS PLpro inhibitor GRL0617 is highly effective in reducing the activity of SARS-2 PLpro and showed high potency and excellent antiviral activity in a SARS-CoV-2 infection model.[16,18] Although GRL-0617 demonstrated good potency, there is a lack of data on its pharmacokinetic profile. GRL-0617 has not yet been tested in clinical trials or in animal studies for its *in vivo* efficacy.

Peptide−drug conjugates (PDCs) are a class of novel molecules widely designed and synthesized for delivering drug payloads.[32,33] In this work, we designed a novel PDC in which the GRL0617 was linked to the sulfonium-tethered peptides derived from PLpro-specific substrate LRGG. This conjugate could covalently label PLpro active site C111. Two conjugates EM-C and EC-M showed a promising *in vitro* IC50 of 7.40 ± 0.37 and 8.63 ± 0.55 μM, respectively. Both conjugates could effectively inhibit anti-ISGylation activities of PLpro in cells, and there is low toxicity of PDC EC-M and EM-C in different cells (Scheme 1).

Scheme 1. Schematic Presentation of PDCs Covalently Targeting SARS-CoV-2 PLpro

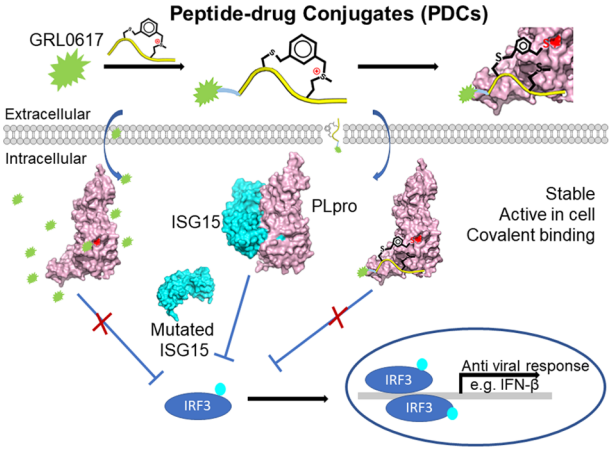

RESULTS AND DISCUSSION

Design of the Novel PDCs Targeting PLpro. Here, we selected GRL0617 as the drug template of PDCs targeting SARS-CoV PLpro-2 (Figure S1). GRL0617 was initially found to inhibit the SARS-CoV PLpro in 2008, with an IC50 of 600 nM.[34] Subsequently, scientists found that GRL0617 is also a promising inhibitor to SARS-CoV-2 PLpro. The targeting range of small molecules is limited to proteins having hydrophobic pockets. Therefore, we intended to design PDCs with a stable covalent peptide to improve GRL0617-targeting specificity and duration of action.

In our previous study, we reported a unique bio-orthogonal reaction in which we tethered a peptide between Cys and Met with a newly formed sulfonium center.[35] When such a peptide recognizes its target and if the protein has a Cys in the vicinity of the interacting interface, the peptide would bind to the protein with high selectivity and efficiency.[36] Based on this method, we first designed a series of sulfonium-tethered peptides to target SARS-CoV-2 PLpro, in which the main catalytic amino acid is the C111 residue. The PLpro recognized a conserved sequence with different substrates including the tetrapeptide LXGG motif found in between viral proteins nsp1 and nsp2, nsp2 and nsp3, and nsp3 and nsp4 for cleavage of the viral polypeptide. Moreover, SARS-CoV-2 PLpro harbors deubiquitinating and deISGylating activities and recognizes the conserved LRGG motif at the C-terminal of ubiquitin or ISG-15 proteins (Figure 1A). Therefore, we designed several sulfonium-tethered peptides derived from the PLpro-specific substrate LXGG motif, which had a warhead to covalently bond with SARS-CoV-2 PLpro. We retained the conserved sequence LRGG and added a cyclic peptide with an on-tether sulfonium center at the C-terminal of LRGG (peptide CM1 and CM2). Then, one residue was mutated to C or M, and another M or C was added to construct the sulfonium-tethered peptides (peptide CM3, CM4, CM5, CM6, CM7, and CM8) (Figure 1B). The peptides were constructed via conventional Fmoc-based solid-phase peptide synthesis (SPPS). Then, peptide cyclization was performed based on reported protocols.[35] The Trt-protected cysteine was deprotected and let to react with di-halogenated linkers on resin. The peptide cleavage from the resin will release the free Met and it will automatically be alkylated to give the cyclized peptides in high yields in the cleavage cocktail (Figure S2).

Sulfonium-Tethered Peptides Covalently Labeled SARS-CoV-2 PLpro *In Vitro*. The peptides were then tested for their covalent bonding ability with SARS-CoV-2 PLpro. Different peptides (10 μM) were reacted with SARS-CoV-2 PLpro (5 μM) in PBS buffer for 1 h, respectively. The linear tetrapeptide LRGG could not label SARS-CoV-2 PLpro because there was no warhead to covalently react with the residue cysteine. Instead, the sulfonium-tethered peptides could covalently label SARS-CoV-2 PLpro. We found that the covalent bond formation reaction efficiency of sulfonium-tethered peptides was generally high, especially for CM1, CM2, CM3, CM4, and CM8. Moreover, the sulfonium-tethered peptides CM1, CM4, and CM8 with warhead designed near to the SARS-CoV-2 PLpro C111 showed a higher covalent reaction efficiency (Figure 1C).

PDCs Covalently Labeled PLpro *In Vitro*. All of the sulfonium-tethered peptides successfully covalently react with SARS-CoV-2 PLpro, and we selected two sulfonium-tethered peptides (CM7 and CM8) to compose PDCs EM-C and EC-M by connecting with GRL0617 (Figures 2A and S3). EM-C and EC-M could covalently bond to SARS-CoV-2 PLpro, while the PDC with linear peptides ELRGG could not bind to SARS-CoV-2 PLpro.

Subsequently, we studied the reaction kinetics and stoichiometry of EC-M and EM-C. SARS-CoV-2 PLpro (5 μM) was left to react with different concentrations of peptide EC-M or EM-C (0, 2.5, 5, 10, 15, 20, and 25 μM) in PBS buffer for 2 h. The reaction showed a dose dependence (Figure 2B,C). Then, peptide EM-C (10 μM) was left to react with SARS-CoV-2 PLpro (5 μM) in PBS buffer for different time periods (0.5, 1, 2, 3, and 4 h). The reaction started within 1 h and the efficiency of the reaction increased with time (Figure 2B,C). The kinetics and stoichiometric study clearly showed the efficiency of the conjugation.

There are eleven cysteine residues (C111, C148, C155, C181, C189, C192, C224, C226, C260, C270, and C284) in SARS-CoV-2 PLpro, while only Cys111 is close to the binding site. We

https://doi.org/10.1021/acs.jmedchem.1c02022
J. Med. Chem. 2022, 65, 876−884

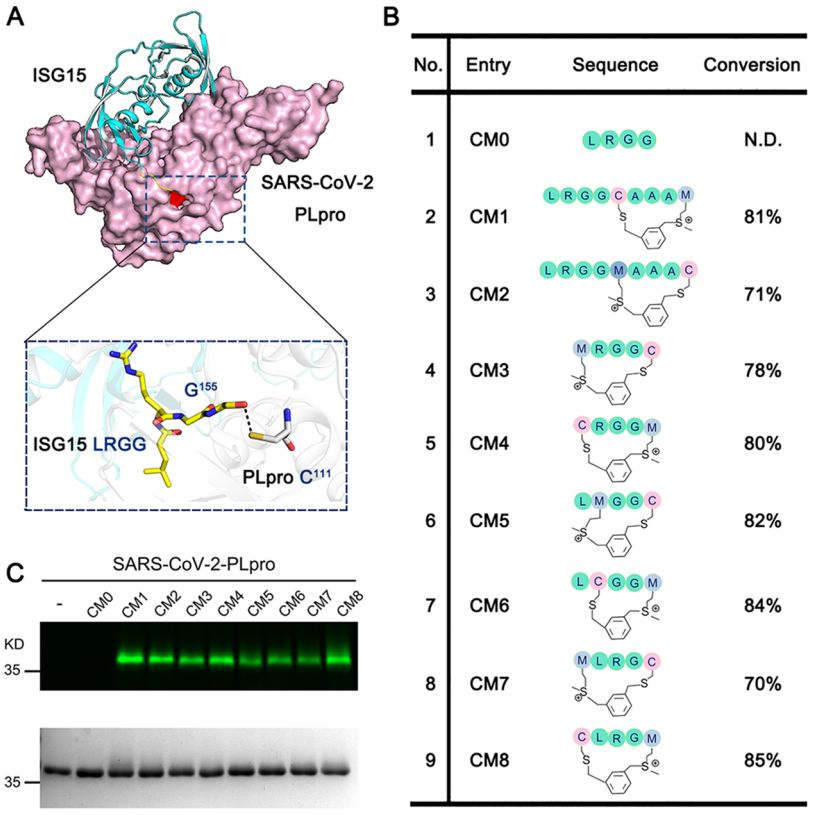

Figure 1. Preparation of sulfonium-tethered peptides targeting SARS-CoV-2 PLpro. (A) Structure of ISG15-bound SARS-CoV-2 PLpro (PDB ID: 6YVA and 6WX4). ISG15 C terminal amino acid LRGG is close to C111 of SARS-CoV-2 PLpro. (B) Sequence and conversion efficiency of the designed sulfonium-tethered peptides. (C) SARS-CoV-2 PLpro-peptide conjugation analysis. The different peptides (10 μM) were mixed with SARS-CoV-2 PLpro (5 μM) in PBS buffer for 1 h.

identified the binding sites of peptide and protein by tandem mass spectrometry. The MS/MS analysis of in-gel digest for EC-M-bound PLpro showed that peptide EC-M bound to several Cys sites of PLpro. Nevertheless, the MS/MS analysis of in-gel digest for EC-M-bound PLpro has shown that covalent conjugation mainly happened on the C111 site because of rich ion fragments and high identification score from C111 (Figure 2D) compared with other two possible sites (Figures S4 and S5). Indeed, we found that mutated PLpro^{C111S} has a much weaker reaction with EM-C than PLpro, confirming a strong selectivity toward C111 (Figure S6). Altogether, the PDCs EC-M and EM-C mainly covalently bind to the C111 on PLpro.

To assess the ability of peptides EM-C and EC-M to label PLpro in a complex proteome environment, 293T cell lysates (300 μg) were spiked with PLpro (5 μM) and then treated with 10 μM FAM-labeled peptides EM-C and EC-M. The gel data showed a clear single fluorescent band with the correct molecular weight indicating a clean and selective conjugation of peptide EM-C and EC-M to PLpro (Figure S7).

Identification of PDCs EC-M and EM-C as an inhibitor for SARS-CoV-2 PLpro. The enzymatic activities of SARS-CoV-2 PLpro were tested using the fluorogenic peptide substrate LRGG-AMC. The sulfonium-tethered peptides without GRL0617 could not efficiently inhibit SARS-CoV-2 PLpro (Figure S8), while the sulfonium-tethered peptide conjugate GRL0617 has a better inhibition ability. Specifically, IC50 values of EM-C and EC-M were 7.40 ± 0.37 and 8.63 ± 0.55 μM, respectively (Figure 3A,B).

Also, we tested the peptide inhibition ability to SARS-CoV PLpro and MERS PLpro. There is a high sequence identity (83%) between the SARS-CoV-2 PLpro and SARS-CoV PLpro. The IC50 value of EM-C against SARS-CoV PLpro was 3.43 ± 0.54 μM, close to GRL0617 (IC50 = 2.60 ± 0.05 μM). Its linear analogue showed weaker inhibition (Figure 3C). The GRL0617, EC-M, EM-C, and ELRGG could not inhibit MERS PLpro (Figure 3D). Both EM-C and EC-M showed better inhibition for SARS-CoV PLpro than SARS-CoV-2 PLpro.

PDC-Inhibited PLpro Regulates IFN Pathways. To investigate the inhibitory effects of EM-C and EC-M on the deISGylation activity of PLpro inside cells, two cell-based methods, anti-ISG15 immunoblotting and luciferase-based IFN-β reporter assay, were performed to test whether EM-C and EC-M could recover the cellular ISGylation level and therefore the host innate immune response by inhibiting PLpro. Consistent with their activities in the enzyme inhibition assays, both EM-C and EC-M can recover the cellular ISGylation level in a dose-dependent manner (Figure 4A), indicating that they can enter cells to inhibit SARS-CoV-2 PLpro. Meanwhile, EC-M showed a higher potency to recover the cellular ISGylation level than EM-C. Consistent with its potency in anti-ISG15 immunoblotting, EC-M can also significantly recover the IFN-β promoter activity suppressed by SARS-CoV-2 PLpro in a dose-dependent manner, suggesting that it has the potential to reactivate the host innate immune response (Figure 4B). However, EM-C did not show significant recovery of the IFN-β promoter activity even at 100 μM, likely due to its relatively low potency to inhibit deISGylation on the cellular level.

Low Toxicity of PDCs EC-M and EM-C. MTT assay was performed with different cell lines to examine peptides' effects on cell proliferation. Peptides were used to treat different cell

https://doi.org/10.1021/acs.jmedchem.1c02022
J. Med. Chem. 2022, 65, 876−884

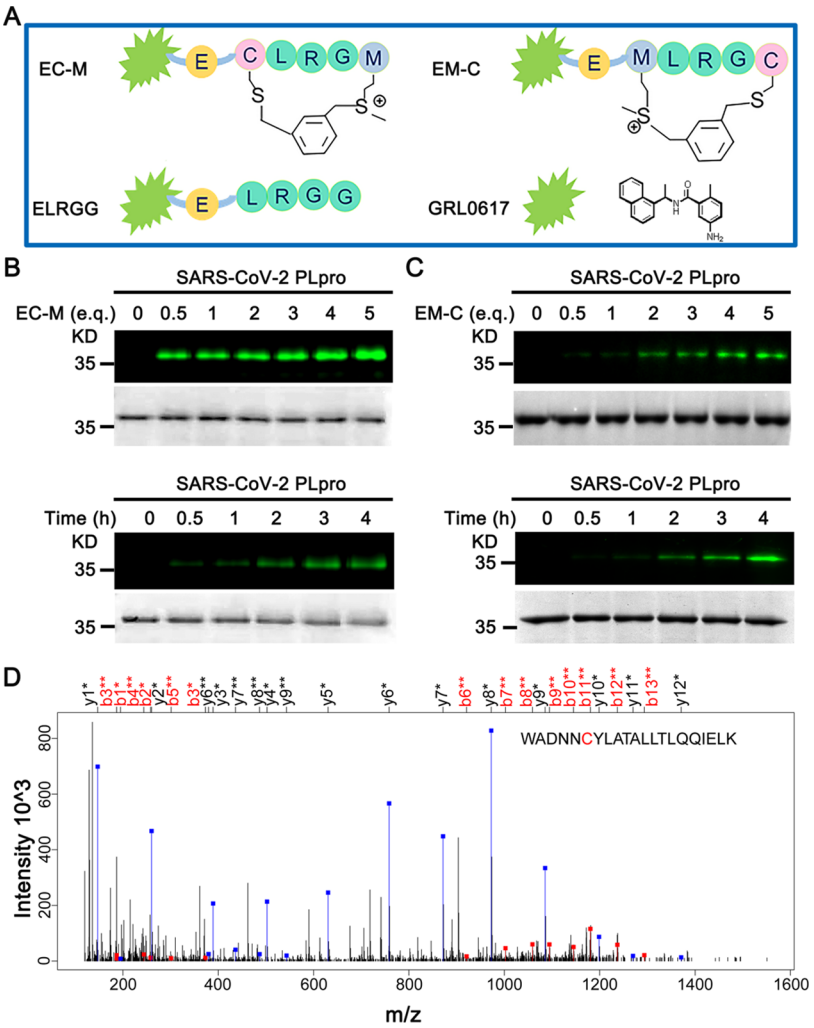

Figure 2. Design and reaction formation of novel PDC targeting SARS-CoV-2 PLpro. (A) Sequence of designed peptide−drug conjugations. (B) Reaction stoichiometric and reaction kinetic study of SARS-CoV-2 PLpro and EC-M. SARS-CoV-2 PLpro (5 μM) reacted with different concentrations of peptide EC-M (0, 2.5, 5, 10, 15, 20, and 25 μM) in PBS buffer for 2 h. Peptide EC-M (10 μM) reacted with SARS-CoV-2 PLpro (5 μM) in PBS buffer for different time periods (0.5, 1, 2, 3, and 4 h). (C) Reaction stoichiometric and reaction kinetic study of SARS-CoV-2 PLpro and EM-C. SARS-CoV-2 PLpro (5 μM) reacted with different concentrations of peptide EM-C (0, 2.5, 5, 10, 15, 20, and 25 μM) in PBS buffer for 2 h. Peptide EM-C (10 μM) reacted with SARS-CoV-2 PLpro (5 μM) in PBS buffer for different time periods (0.5, 1, 2, 3, and 4 h). (D) MS/MS analysis determines that Cys111 is the modification site.

lines at different concentrations for 24 h. The GRL0617 and PDCs EC-M and EM-C showed no growth inhibition of both A549 and 293T (Figure 4C). The nonspecific toxicity of these peptide inhibitors was further excluded using the hemolysis assay (Figure 4D).

CONCLUSIONS

COVID-19 pandemic has emerged as a global health threat due to its high transmission and deaths. Novel designs of antiviral agents may help in battling against SARS-CoV-2 and other virus-related pandemics in the future.

In our report, we designed a novel PDC to target SARS-CoV-2 PLpro. The novel PDC, in which GRL0617 was linked to the sulfonium-tethered peptides derived from PLpro-specific substrate LRGG, could covalently label PLpro active site C111. The PDCs EM-C and EC-M showed a promising *in vitro* IC50 of 7.40 ± 0.37 and 8.63 ± 0.55 μM, respectively. Then, we also evaluated the ability of PDCs to inhibit anti-ISGylation activities of PLpro in cells. Notably, these conjugates significantly reduced GRL0617's cytotoxicity (Figure S9). The permeability is a crucial factor for their druggability. We found that the PDCs EC-M, EM-C, and ELRGG had a better cellular uptake ability, compared to the positive control peptide TAT (Figure S10).

Furthermore, we found that PDCs EC-M and EM-C are also covalently bound to SARS-CoV PLpro and MERS PLpro (Figure S11). The PDCs EM-C and EC-M showed an *in vitro* IC50 of 3.43 ± 0.54 and 16.38 ± 0.81 μM to SARS-CoV PLpro, respectively. Both the two PDCs could recover the cellular ISGylation level suppressed by SARS-CoV-2 PLpro in a dose-dependent manner in the anti-ISG15 immunoblotting assay, and EC-M also showed the recovery of IFN-β promoter activity on the cellular level. These results suggested that EC-M can potentially not only interfere with SARS-CoV-2 replication by inhibiting one of its essential proteases but also reactivate the host innate immune response against viral infection.

The results represent a novel attempt to design covalent PDCs, which showed intriguing activities and a significantly reduced cytotoxicity. This PDC-designing strategy could be

https://doi.org/10.1021/acs.jmedchem.1c02022
J. Med. Chem. 2022, 65, 876−884

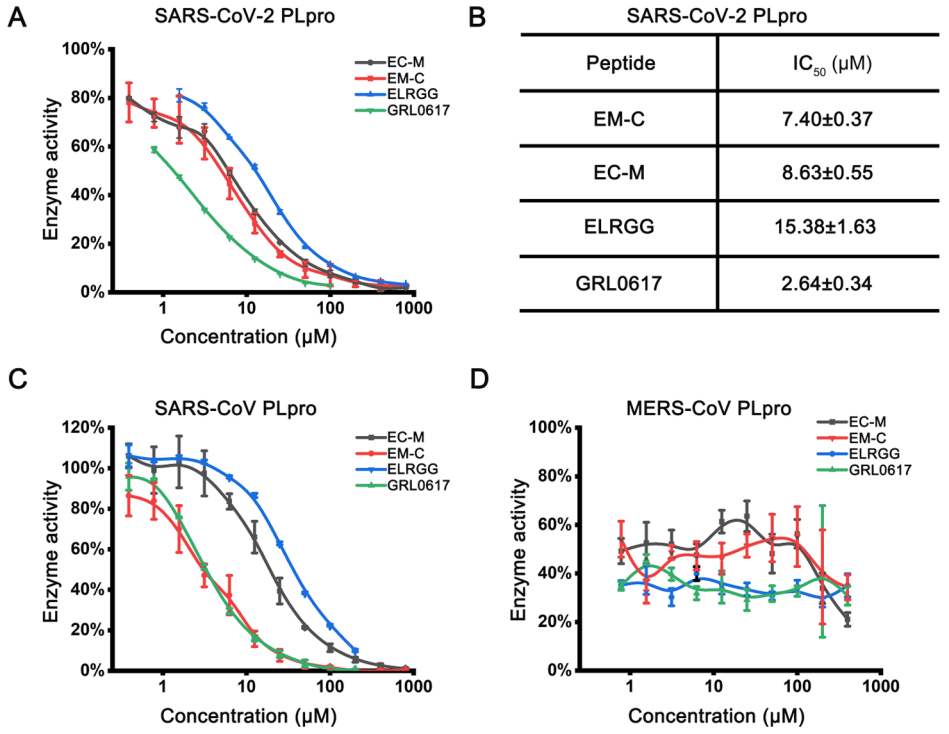

Figure 3. Enzymatic activities of PLpro were inhibited by different PDCs or GRL0617. (A) Enzymatic activity of SARS-CoV-2 PLpro was inhibited by different PDCs or GRL0617. The activity assay was performed using the peptide LRGG-ACC as a substrate. Error bars represent standard errors of mean of at least three independent measurements. (B) IC50 of different PDCs or GRL0617 in SARS-CoV-2 PLpro. IC50 of EM-C was 7.40 ± 0.37 μM. IC50 of EC-M was 8.63 ± 0.55 μM. IC50 of ELRGG was 15.38 ± 1.63 μM. IC50 of GRL0617 was 2.64 ± 0.34 μM. (C) Enzymatic activity of SARS-CoV PLpro was inhibited by different PDCs or GRL0617. (D) Enzyme activity of MERS PLpro was inhibited by different PDCs or GRL0617.

applied to targeting other important proteins for therapeutic applications.

EXPERIMENTAL SECTION

Materials and Methods. *Materials.* All reagents (amino acids and resins) used for SPPS were purchased from Aladdin Co., GL Biochem CO., Shanghai Hanhong Chemical Co., or Energy Chemical Co. All solvents were purchased from Cantotech Chemicals Co. or J&K Scientific Co. They were used without further purification unless otherwise stated. The reagents used for biological assays were purchased from Sigma Aldrich and Thermo Fisher. Cells were purchased through ATCC and cultured according to ATCC guidelines.

Synthesis and Purification of Sulfonium-Tethered Peptides. Peptides were assembled on Rink Amide MBHA resin via standard manual 9-fluorenylmethyloxycarbonyl (Fmoc) SPPS. For N-terminal-acetylated peptides, the N-terminus was acetylated in DMF with Ac2O and DIPEA (1:0.4) for 30 min twice. For 5-carboxyfluorescein (FAM)-labeling peptides, the peptide assembly continued to incorporate the N-terminal residue Fmoc-βAla-OH before FAM, FAM (7.0 equiv) was dissolved in DMF, followed by benzotriazole-1-yl-oxytripyrrolidino-phosphonium hexafluorophosphate (PyBOP, 3.0 equiv), 1-hydroxybenzotriazole (HOBT, 3.0 equiv), and 4-methylmorpholinein (NMM, 6.0 equiv) for 12 h. For circular peptides, they were synthesized with a previous method reported by Wang et al.[35] Peptides were purified by analytic reverse-phase HPLC (Shimadzu LC-20AT: 4.6 × 250 mm, 220 nm and 254 nm) and analyzed by LC−MS (AB SCIEX Elite QSTAR or Shimazu LC−MS 2020) (Figure S1). The peptide purity is >95%.

Synthesis and Purification of PDCs. The synthetic route figures of PDCs were given in the supplementary methods (Figure S2). First, the sulfonium-tethered peptides were assembled on Rink Amide MBHA resin via standard manual Fmoc SPPS. The sulfonium-tethered peptides were linked to GRL0617 through the linker glutamic acid. Fmoc-Glu (OAll)-OH (2.0 equiv according to the initial loading of the resin) and HATU (2.0 equiv) were dissolved in DMF, followed by DIPEA (4.0 equiv). The mixture was preactivated for 1 min and added to the resin for 1 h with N_2 bubbling. The resin was washed sequentially with DCM, DMF (5×), and methanol (5×) and then dried under a stream of nitrogen for the next step. The allyl ester and allyl carbamate were removed using Pd $(PPh_3)_4$ (0.1 equiv) and *N*,*N*-dimethylbarbituric acid (4 equiv) in DCM for 2 h. Then, the GRL0617 (5.0 equiv according to initial loading of the resin), HOBT (3.0 equiv), and PyBOP (3.0 equiv) were dissolved in DMF, followed by NMM (6.0 equiv). The mixture was added to the resin for 1 h with N2 bubbling. The peptides were N-terminal-acetylated or FAM-labeled by the previous methods. Also, the circular peptides were synthesized with a previous method reported by Wang et al. PDCs were purified by analytic reverse-phase HPLC (Shimadzu LC-20AT: 4.6 × 250 mm, 220 nm and 254 nm) and analyzed by LC−MS (AB SCIEX Elite QSTAR or Shimazu LC−MS 2020). The purity of PDCs is >95%.

Recombinant Protein Expression and Purification. Coding sequences of SARS-CoV/MERS-CoV/SARS-CoV-2 PLpro were codon-optimized, synthesized, and cloned into a pET28a vector. A protease activity-abolished variant of SARS-CoV-2 PLpro (C111S) was constructed and also cloned into a pET28a vector. For SARS-CoV-2 PLpro, the expressing plasmid was transformed into competent *Escherichia coli* BL21 (DE3) cells. A single colony was picked and inoculated in 5 mL of LB supplemented with 50 μg/mL kanamycin at 37 °C. The 5 mL inoculum was added to 1 L LB broth with kanamycin. The cells were allowed to grow to an optical density of 0.6 at 600 nm at 37 °C and 180 rpm and were induced with 0.5 mM isopropyl-beta-D-thiogalactopyranoside (IPTG). The induced cells were incubated overnight at 16 °C and 130 rpm. The cells were harvested and resuspended in lysis buffer [50 mM Tris, 300 mM NaCl, 10 mM imidazole, and 5 mM 2-hydroxy-1-ethanethiol (β-ME), pH 8.5] and then lysed by sonication. The cell debris was removed by centrifugation at 15,000 rpm for 60 min. The supernatant was added to a Ni-NTA column, and bound proteins were eluted with buffer B (50 mM Tris, 300 mM NaCl, and 250 mM imidazole, pH 8.5). The elution fractions were finally loaded onto gel filtration (Superdex200, GE Healthcare) with buffer C (20 mM Tris, 100 mM NaCl, and 1 mM DTT, pH 7.4).

https://doi.org/10.1021/acs.jmedchem.1c02022
J. Med. Chem. 2022, 65, 876−884

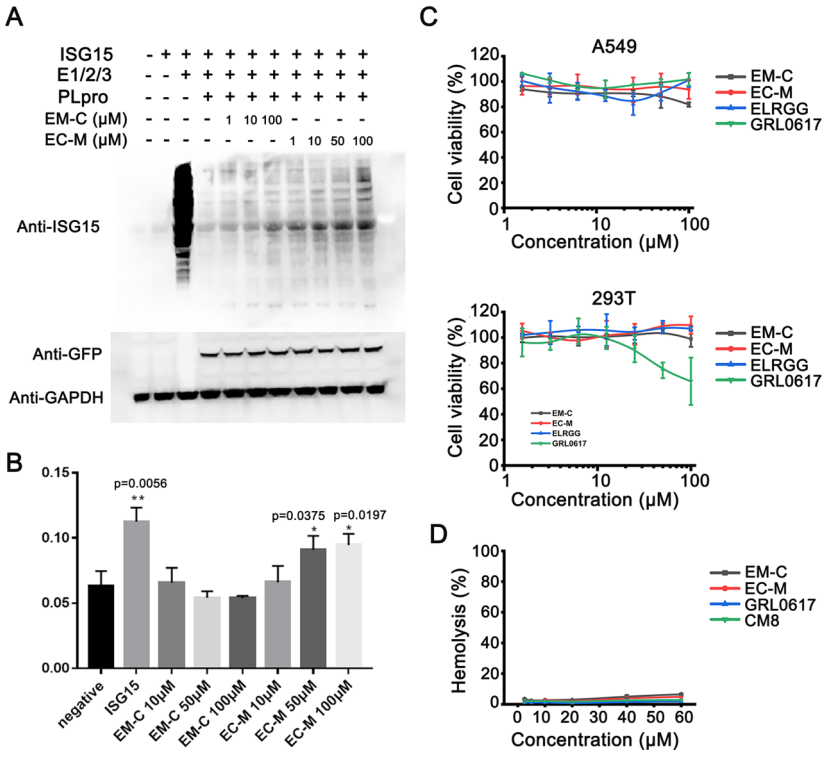

Figure 4. EC-M and EM-C can recover the antiviral activity of ISG15 according to cell-based assays. (A) Immunoblotting for detection of ISGylation with or without EC-M or EM-C treatment at various concentrations, with the plasmids encoding ISG15, E1/E2/E3 ubiquitin ligases, and GFP-PLpro in combination. (B) Reduced suppression of IFN-β promoter activity by SARS-CoV-2 PLpro in the presence of EC-M and EM-C according to luciferase-based IFN-β reporter assay. The negative control is treated with a blank plasmid. The sample treated with ISG15 expressed that the plasmid is selected as a positive control, and its IFN-β promoter activity is set as 100% percentage of effect. Other samples are presented by scaling to the positive control. Significance relative to the negative control was calculated by an unpaired two-tailed Student's *t*-test and labeled above the histogram bars. (C) Viability of A549 and 293T treating with different PDCs or GRL0617. The cells were incubated with 1.56, 3.13, 6.25, 12.5, 25, 50, and 100 μM different PDCs or GRL0617 for 24 h. (D) Hemolysis assays were performed to assess the erythrocyte toxicity of PDC inhibitors. Both PDCs with cyclic peptides and linear peptides had low toxicity to erythrocyte at the concentration of 60 μM. Error bars represent standard errors of mean of at least three independent measurements.

The proteins fractions were concentrated using a 10 kDa MWCO concentrator (Amicon Millipore) and stored at −80 °C. The expression and purification protocols of SARS-CoV PLpro, MERS PLpro, and SARS-CoV-2 PLproC111S were the same as the one for SARS-CoV-2 PLpro.

In Vitro Protein-Peptide Covalent Conjugation Assay. To measure the conjugation reactions, first, the different FAM-labeling peptides (10 μM) were reacted with PLpro (5 μM) in PBS buffer. The mixture was incubated for 1 h and sent for SDS gel analysis. Then, different concentrations of peptide EM-C or EC-M (0, 2.5, 5, 10, 15, 20, and 25 μM) were incubated with protein PLpro (5 μM) in PBS buffer (pH 7.4, 37 °C) for 1 h and then analyzed through 15% SDS-PAGE. The peptide EM-C or EC-M (10 μM) was incubated with protein PLpro (5 μM) in PBS buffer (pH 7.4, 37 °C) for different time periods (0.5, 1, 2, 3, and 4 h) and then analyzed through 15% SDS-PAGE.

In-Gel Trypsin Digestion. EC-M (30 μM) was incubated with protein PLpro (5 μM) in Tris buffer at 37 °C for 4 h. The gel bands corresponding to the conjugation were removed from 15% SDS-PAGE after electrophoresis. Then, the gels were destained by a solution of ammonium bicarbonate: acetonitrile. The gel pieces were incubated with trypsin overnight at 16 °C. The digest was extracted in 50% acetonitrile with 0.5% formic acid and combined with the trypsin digestion supernatant. The treated samples were used for MS/MS analysis.

PLpro Enzyme Activity Assays and IC50 Determination. PLpro activity was monitored using the substrate peptide-ACC (Ac-Leu-Arg-Gly-Gly-ACC, synthesized by solid-phase synthesis). SARS-CoV-2 PLpro and peptide were incubated for 1 h at 37 °C in assay buffer before the final substrate was added. The assay buffer contained 50 mM HEPES, pH 7.4, 0.1 mg/mL BSA, and 5 mM DTT. The SARS-CoV-2 PLpro concentration was 0.1 μM, the final substrate concentration was 1 μM, and the peptide inhibitor concentration was diluted down from 800 μM. Substrate hydrolysis was measured for 30 min at 355 nm (excitation) and 460 (emission) at least three times. The data were fitted using Origin 2020b, and the IC50 value was determined.

Cell Lines and Culture. Human lung adenocarcinoma A549 cells were cultured in RPMI-1640 supplemented with 10% (v/v) FBS and penicillin/streptomycin (100 μg/mL) at 37 °C and 5% CO_2. Human kidney cells 293T cells were cultured in DMEM with 10% (v/v) FBS (Gibco) and penicillin/streptomycin (100 μg/mL) at 37 °C and 5% CO_2. Human colorectal adenocarcinoma cells HCT116 cells were cultured in RPMI-1640 supplemented with 10% (v/v) FBS and penicillin/streptomycin (100 μg/mL) at 37 °C and 5% CO_2. All reagents were purchased from Gibco. All these cells were maintained in a humidified incubator containing 5% CO_2 at 37 °C.

Cell Viability Assay by MTT Assays. The cells were cultured in each well of the 96-well plates overnight and then treated with peptides in 100 μL of medium containing 5% FBS for 24 h. A total of 20 μL of MTT reagent (5 mg/mL) was added and the cells were incubated at 37 °C for 4 h. DMSO (150 μL) was added and shaken for 10 min. The control group was treated with the same amount of DMSO without peptides. Absorbance was detected at a wavelength of 490 nm using a microplate reader (Bio-Rad).

Immunoblotting for Detection of ISGylation. To detect the intracellular ISGylation level, HEK293T cells were co-transfected with plasmids encoding Myc-tagged ISG15, E1/E2/E3 ubiquitin ligases, and SARS-CoV2 PLpro fused with EGFP. After transfection, the cells were incubated in DMEM with 5% FBS and PDCs (EC-M or

https://doi.org/10.1021/acs.jmedchem.1c02022
J. Med. Chem. 2022, 65, 876−884

EM-C) for 24 h at 37 °C. Then, the cells were washed with PBS and harvested using the 1× passive lysis buffer (Promega, 11, E1941), and the extracted protein concentrations were quantitated using the BCA method. For each sample, 30 μg of the protein was loaded for SDS-PAGE and transferred to the PVDF membrane afterward. Western blotting was performed using the following primary antibody dilutions: 1:1000 for anti-ISG15 (CST, 2758), 1:1000 for anti-GFP (CST, 2956), 1:1000 for anti-GAPDH (Biodragon, B1034) antibodies, and 1:1000 for HRP-conjugated secondary antibody (Biodragon, BF03008) dilution. The membrane was visualized using the ECL substrate (Beyotime, P0018AFT) with a ChemiDoc MP Imaging System (Bio-Rad).

Luciferase-Based IFN-β Reporter Assay. In the luciferase-based IFN-β reporter assay, the effect of PDCs on the suppression of IFN-β promoter activity by SARS-CoV2 PLpro was investigated following the same protocol as ref 31. Briefly speaking, HEK293T cells were co-transfected with plasmids encoding Renilla luciferase as a reference, Firefly luciferase is driven by an IFN-β promoter, MAVS, to activate IFN-β promoter and SARS-CoV2 PLpro. Firefly and Renilla luciferase activities were measured using the dual-Luciferase reporter assay system (Promega, E1910), and the IFN-β promoter activity was reflected by Firefly luciferase activity normalized by Renilla luciferase activity. Experiments were performed in three biological replicates; unpaired two-tailed Student's *t*-test was employed to determine the statistical significance.

Hemolysis Assays. Fresh mouse erythrocytes were collected and centrifuged at 1500 rpm for 10 min. Then, the cells were washed four times and resuspended in PBS to a final density of 10^8/mL. A serial dilution of peptides, different PDCs, or GRL0617 was added starting at 60 μM and incubated at 37 °C for 1.5 h. Then, erythrocytes were centrifuged at 6000 rpm for 10 min. The absorbance of the supernatant at 570 nm was measured using a microplate reader (PerkinElmer, Envision) to monitor the release of hemoglobin. 0.1% Triton X-100 and PBS were employed as positive and negative controls, respectively. The calculation formula of the hemolysis rate is % hemolysis = [(A576 nm of sample − A576 nm of negative control)/(A576 nm of positive control − A576 nm of negative control)] × 100.

■ ASSOCIATED CONTENT

Supporting Information

The Supporting Information is available free of charge at https://pubs.acs.org/doi/10.1021/acs.jmedchem.1c02022.

Synthesis of GRL0617; covalent conjugation assay of mutated PLpro^{C111S} with PDC EM-C *in vitro*; flow cytometry; synthetic route of GRL0617; synthesis of sulfonium-tethered peptides; synthesis of PDCs; MS/MS analysis of protein PLpro and EC-M conjugation at C181; MS/MS analysis of protein PLpro and EC-M conjugation at C192; covalent conjugation assay of mutated PLproC111S with PDCs EM-C *in vitro*; 293T cell lysates with 5 μM SARS-CoV-2 PLpro; enzymatic activity of SARS-CoV-2 PLpro; MTT of GRL0617 in different cells; cellular uptake of PDCs; reaction study of SARS-CoV-2 PLpro, SARS-CoV PLpro, MERS PLpro, and EC-M; mass statistics data for the peptides and structure of unnatural amino acids; and LC−MS spectra of peptides used in the manuscript (PDF)

Molecular formula strings of SARS-CoV PLpro and SARS-CoV-2 PLpro (CSV)

■ AUTHOR INFORMATION

Corresponding Authors

Jian Zhan − *Institute for Systems and Physical Biology, Shenzhen Bay Laboratory, Shenzhen, Guangdong 518032, China*; Email: zhanjian@szbl.ac.cn

Feng Yin − *State Key Laboratory of Chemical Oncogenomics, Guangdong Provincial Key Laboratory of Chemical Genomics, School of Chemical Biology and Biotechnology, Peking University Shenzhen Graduate School, Shenzhen 518055, China; Pingshan Translational Medicine Center, Shenzhen Bay Laboratory, Shenzhen 518118, China*; Email: yinfeng@pkusz.edu.cn

Zigang Li − *State Key Laboratory of Chemical Oncogenomics, Guangdong Provincial Key Laboratory of Chemical Genomics, School of Chemical Biology and Biotechnology, Peking University Shenzhen Graduate School, Shenzhen 518055, China; Pingshan Translational Medicine Center, Shenzhen Bay Laboratory, Shenzhen 518118, China*; orcid.org/0000-0002-3630-8520; Email: lizg@pkusz.edu.cn

Authors

Na Liu − *State Key Laboratory of Chemical Oncogenomics, Guangdong Provincial Key Laboratory of Chemical Genomics, School of Chemical Biology and Biotechnology, Peking University Shenzhen Graduate School, Shenzhen 518055, China; Pingshan Translational Medicine Center, Shenzhen Bay Laboratory, Shenzhen 518118, China*

Yichi Zhang − *State Key Laboratory of Chemical Oncogenomics, Guangdong Provincial Key Laboratory of Chemical Genomics, School of Chemical Biology and Biotechnology, Peking University Shenzhen Graduate School, Shenzhen 518055, China*

Yingshou Lei − *Institute for Systems and Physical Biology, Shenzhen Bay Laboratory, Shenzhen, Guangdong 518032, China*

Rui Wang − *Pingshan Translational Medicine Center, Shenzhen Bay Laboratory, Shenzhen 518118, China*; orcid.org/0000-0003-3830-4133

Meimiao Zhan − *State Key Laboratory of Chemical Oncogenomics, Guangdong Provincial Key Laboratory of Chemical Genomics, School of Chemical Biology and Biotechnology, Peking University Shenzhen Graduate School, Shenzhen 518055, China*

Jianbo Liu − *Pingshan Translational Medicine Center, Shenzhen Bay Laboratory, Shenzhen 518118, China*

Yuhao An − *Pingshan Translational Medicine Center, Shenzhen Bay Laboratory, Shenzhen 518118, China*

Yaoqi Zhou − *Institute for Systems and Physical Biology, Shenzhen Bay Laboratory, Shenzhen, Guangdong 518032, China*; orcid.org/0000-0002-9958-5699

Complete contact information is available at: https://pubs.acs.org/10.1021/acs.jmedchem.1c02022

Author Contributions

#N.L., Y.Z., and Y.L. contributed equally to this work. J.Z., F.Y., and Z.L. planned the study. N.L., Y.Z., Y.L., R.W., M.Z., J.L., and Y.A. performed the research. Y.Z., J.Z., F.Y., and Z.L. wrote the manuscript with feedback from all authors. All authors have given approval to the final version of the manuscript.

Notes

The authors declare no competing financial interest.

■ ACKNOWLEDGMENTS

We acknowledge financial support from the National Natural Science Foundation of China grants 21778009 and 21977010; National Key Research and Development Program "Synthetic Biology" Key Special Project of China, 2018YFA0902504; the

Natural Science Foundation of Guangdong Province, 2020A1515011544 and 2020A1515010522; and the Shenzhen Science and Technology Innovation Committee, RCJC20200714114433053, JCYJ20180508152213145 5, and JCYJ20200109140406047. We acknowledge financial support from Beijing National Laboratory of Molecular Science Open Grant BNLMS20160112, Shenzhen-Hong Kong Institute of Brain Science-Shenzhen Fundamental Research Institutions Grant 2019SHIBS0004, Shenzhen Bay Laboratory Major Program S201101001, and Shenzhen Bay Laboratory Open Program SZBL2021080601010. This work is supported by High-Performance Computing Platform of Peking University. We would like to thank Dr. Hao Huang lab at Peking University Shenzhen Graduate School for the plasmids of ISGylation assay.

■ ABBREVIATIONS

β-ME, 2-hydroxy-1-ethanethiol; COVID-19, coronavirus disease 2019; FAM, 5-carboxyfluorescein; Fmoc, 9-fluorenylmethyloxycarbonyl; HOBT, 1-hydroxybenzotriazole; IPTG, isopropyl-beta-D-thiogalactopyranoside; ISG15, interferon-stimulated gene 15; MERS, Middle East respiratory syndrome; NMM, 4-methylmorpholinein; PDCs, peptide−drug conjugates; PLpro, papain-like protease; PyBOP, benzotriazole-1-yl-oxy-tripyrrolidinophosphonium hex-afluorophosphate; SARS-CoV-2, severe acute respiratory syndrome coronavirus 2; SPPS, solid-phase peptide synthesis; WHO, World Health Organization

■ REFERENCES

(1) Hu, B.; Guo, H.; Zhou, P.; Shi, Z.-L. Characteristics of SARS-CoV-2 and COVID-19. *Nat. Rev. Microbiol.* **2021**, *19*, 141−154.

(2) Huang, C.; Wang, Y.; Li, X.; Ren, L.; Zhao, J.; Hu, Y.; Zhang, L.; Fan, G.; Xu, J.; Gu, X.; Cheng, Z.; Yu, T.; Xia, J.; Wei, Y.; Wu, W.; Xie, X.; Yin, W.; Li, H.; Liu, M.; Xiao, Y.; Gao, H.; Guo, L.; Xie, J.; Wang, G.; Jiang, R.; Gao, Z.; Jin, Q.; Wang, J.; Cao, B. Clinical Features of Patients Infected with 2019 Novel Coronavirus in Wuhan, China. *Lancet* **2020**, *395*, 497−506.

(3) Ludwig, S.; Zarbock, A. Coronaviruses and SARS-CoV-2: A Brief Overview. *Anesth. Analg.* **2020**, *131*, 93−96.

(4) World Health Organization. *Coronavirus Disease (COVID-2019) Situation Reports*. https://www.who.int/emergencies/diseases/novel-coronavirus-2019/situation-reports (WHO, 2021).

(5) Ahn, D.-G.; Shin, H.-J.; Kim, M.-H.; Lee, S.; Kim, H.-S.; Myoung, J.; Kim, B.-T.; Kim, S.-J. Current Status of Epidemiology, Diagnosis, Therapeutics, and Vaccines for Novel Coronavirus Disease 2019 (COVID-19). *J. Microbiol. Biotechnol.* **2020**, *30*, 313−324.

(6) Asselah, T.; Durantel, D.; Pasmant, E.; Lau, G.; Schinazi, R. F. COVID-19: Discovery, Diagnostics and Drug development. *J. Hepatol.* **2021**, *74*, 168−184.

(7) Beyrampour-Basmenj, H.; Milani, M.; Ebrahimi-Kalan, A.; Ben Taleb, Z.; Ward, K. D.; Dargahi Abbasabad, G.; Aliyari-Serej, Z.; Ebrahimi Kalan, M. An Overview of the Epidemiologic, Diagnostic and Treatment Approaches of COVID-19: What do We Know? *Public Health Rev.* **2021**, *42*, 1604061.

(8) Fathizadeh, H.; Afshar, S.; Masoudi, M. R.; Gholizadeh, P.; Asgharzadeh, M.; Ganbarov, K.; Köse, Ş.; Yousefi, M.; Kafil, H. S. SARS-CoV-2 (Covid-19) Vaccines Structure, Mechanisms and Effectiveness: A Review. *Int. J. Biol. Macromol.* **2021**, *188*, 740−750.

(9) Rehman, S. U.; Rehman, S. U.; Yoo, H. H. COVID-19 Challenges and Its Therapeutics. *Biomed. Pharmacother.* **2021**, *142*, 112015.

(10) Raman, R.; Patel, K. J.; Ranjan, K. COVID-19: Unmasking Emerging SARS-CoV-2 Variants, Vaccines and Therapeutic Strategies. *Biomolecules* **2021**, *11*, 993.

(11) Imran, M.; Kumar Arora, M.; Asdaq, S. M. B.; Khan, S. A.; Alaqel, S. I.; Alshammari, M. K.; Alshehri, M. M.; Alshrari, A. S.; Mateq Ali, A.; Al-Shammeri, A. M.; Alhazmi, B. D.; Harshan, A. A.; Alam, M. T.; Abida, A. Discovery, Development, and Patent Trends on Molnupiravir: A Prospective Oral Treatment for COVID-19. *Molecules* **2021**, *26*, 5795.

(12) Painter, W. P.; Holman, W.; Bush, J. A.; Almazedi, F.; Malik, H.; Eraut, N.; Morin, M. J.; Szewczyk, L. J.; Painter, G. R. Human Safety, Tolerability, and Pharmacokinetics of Molnupiravir, a Novel Broad-Spectrum Oral Antiviral Agent with Activity Against SARS-CoV-2. *Antimicrob. Agents Chemother.* **2021**, *65*, No. e02428.

(13) Menéndez-Arias, L. Decoding Molnupiravir-Induced Mutagenesis in SARS-CoV-2. *J. Biol. Chem.* **2021**, *297*, 100867.

(14) Pan, H.; Peto, R.; Henao-Restrepo, A. M.; Preziosi, M. P.; Sathiyamoorthy, V.; Abdool Karim, Q.; Alejandria, M. M.; Hernandez Garcia, C.; Kieny, M. P.; Malekzadeh, R.; Murthy, S.; Reddy, K. S.; Roses Periago, M.; Abi Hanna, P.; Ader, F.; Al-Bader, A. M.; Alhasawi, A.; Allum, E.; Alotaibi, A.; Alvarez-Moreno, C. A.; Appadoo, S.; Asiri, A.; Aukrust, P.; Barratt-Due, A.; Bellani, S.; Branca, M.; Cappel-Porter, H. B. C.; Cerrato, N.; Chow, T. S.; Como, N.; Eustace, J.; Garcia, P. J.; Godbole, S.; Gotuzzo, E.; Griskevicius, L.; Hamra, R.; Hassan, M.; Hassany, M.; Hutton, D.; Irmansyah, I.; Jancoriene, L.; Kirwan, J.; Kumar, S.; Lennon, P.; Lopardo, G.; Lydon, P.; Magrini, N.; Maguire, T.; Manevska, S.; Manuel, O.; McGinty, S.; Medina, M. T.; Mesa Rubio, M. L.; Miranda-Montoya, M. C.; Nel, J.; Nunes, E. P.; Perola, M.; Portoles, A.; Rasmin, M. R.; Raza, A.; Rees, H.; Reges, P. P. S.; Rogers, C. A.; Salami, K.; Salvadori, M. I.; Sinani, N.; Sterne, J. A. C.; Stevanovikj, M.; Tacconelli, E.; Tikkinen, K. A. O.; Trelle, S.; Zaid, H.; Rottingen, J. A.; Swaminathan, S.; WHO Solidarity Trial Consortium. Repurposed Antiviral Drugs for Covid-19 - Interim WHO Solidarity Trial Results. *N. Engl. J. Med.* **2021**, *384*, 497−511.

(15) Yan, F.; Gao, F. An Overview of Potential Inhibitors Targeting Non-Structural Proteins 3 (PL(pro) and Mac1) and 5 (3CL(pro)/M(pro)) of SARS-CoV-2. *Comput. Struct. Biotechnol. J.* **2021**, *19*, 4868−4883.

(16) Shin, D.; Mukherjee, R.; Grewe, D.; Bojkova, D.; Baek, K.; Bhattacharya, A.; Schulz, L.; Widera, M.; Mehdipour, A. R.; Tascher, G.; Geurink, P. P.; Wilhelm, A.; van der Heden van Noort, G. J.; Ovaa, H.; Müller, S.; Knobeloch, K.-P.; Rajalingam, K.; Schulman, B. A.; Cinatl, J.; Hummer, G.; Ciesek, S.; Dikic, I. Papain-Like Protease Regulates SARS-CoV-2 Viral Spread and Innate Immunity. *Nature* **2020**, *587*, 657−662.

(17) Rut, W.; Lv, Z.; Zmudzinski, M.; Patchett, S.; Nayak, D.; Snipas, S. J.; El Oualid, F.; Huang, T. T.; Bekes, M.; Drag, M.; Olsen, S. K. Activity Profiling and Crystal Structures of Inhibitor-Bound SARS-CoV-2 Papain-Like Protease: A Framework for Anti-COVID-19 Drug Design. *Sci. Adv.* **2020**, *6*, No. eabd4596.

(18) Fu, Z.; Huang, B.; Tang, J.; Liu, S.; Liu, M.; Ye, Y.; Liu, Z.; Xiong, Y.; Zhu, W.; Cao, D.; Li, J.; Niu, X.; Zhou, H.; Zhao, Y. J.; Zhang, G.; Huang, H. The Complex Structure of GRL0617 and SARS-CoV-2 PLpro Reveals a Hot Spot for Antiviral Drug Discovery. *Nat. Commun.* **2021**, *12*, 488.

(19) Gao, X.; Qin, B.; Chen, P.; Zhu, K.; Hou, P.; Wojdyla, J. A.; Wang, M.; Cui, S. Crystal Structure of SARS-CoV-2 Papain-like Protease. *Acta Pharm. Sin. B* **2021**, *11*, 237−245.

(20) Lim, K. P.; Ng, L. F. P.; Liu, D. X. Identification of a Novel Cleavage Activity of the First Papain-like Proteinase Domain Encoded by Open Reading Frame 1a of The Coronavirus Avian Infectious Bronchitis Virus and Characterization of The Cleavage Products. *J. Virol.* **2000**, *74*, 1674−1685.

(21) Harcourt, B. H.; Jukneliene, D.; Kanjanahaluethai, A.; Bechill, J.; Severson, K. M.; Smith, C. M.; Rota, P. A.; Baker, S. C. Identification of Severe Acute Respiratory Syndrome Coronavirus Replicase Products and Characterization of Papain-Like Protease Activity. *J. Virol.* **2004**, *78*, 13600−13612.

(22) Barretto, N.; Jukneliene, D.; Ratia, K.; Chen, Z.; Mesecar, A. D.; Baker, S. C. The Papain-like Protease of Severe Acute Respiratory Syndrome Coronavirus has Deubiquitinating Activity. *J. Virol.* **2005**, *79*, 15189−15198.

(23) Frieman, M.; Ratia, K.; Johnston, R. E.; Mesecar, A. D.; Baric, R. S. Severe Acute Respiratory Syndrome Coronavirus Papain-like Protease Ubiquitin-like Domain and Catalytic Domain Regulate

Antagonism of IRF3 and NF-kappaB Signaling. *J. Virol.* **2009**, *83*, 6689−6705.
(24) Devaraj, S. G.; Wang, N.; Chen, Z.; Chen, Z.; Tseng, M.; Barretto, N.; Lin, R.; Peters, C. J.; Tseng, C.-T. K.; Baker, S. C.; Li, K. Regulation of IRF-3-dependent Innate Immunity by The Papain-Like Protease Domain of The Severe Acute Respiratory Syndrome Coronavirus. *J. Biol. Chem.* **2007**, *282*, 32208−32221.
(25) Bailey-Elkin, B. A.; Knaap, R. C. M.; Johnson, G. G.; Dalebout, T. J.; Ninaber, D. K.; van Kasteren, P. B.; Bredenbeek, P. J.; Snijder, E. J.; Kikkert, M.; Mark, B. L. Crystal Structure of The Middle East Respiratory Syndrome Coronavirus (MERS-CoV) Papain-like Protease Bound to Ubiquitin Facilitates Targeted Disruption of Deubiquitinating Activity to Demonstrate Its Role in Innate Immune Suppression. *J. Biol. Chem.* **2014**, *289*, 34667−34682.
(26) Calistri, A.; Munegato, D.; Carli, I.; Parolin, C.; Palù, G. The Ubiquitin-conjugating System: Multiple Roles in Viral Replication and Infection. *Cells* **2014**, *3*, 386−417.
(27) Mielech, A. M.; Kilianski, A.; Baez-Santos, Y. M.; Mesecar, A. D.; Baker, S. C. MERS-CoV Papain-like Protease Has DeISGylating and Deubiquitinating Activities. *Virology* **2014**, *450*−*451*, 64−70.
(28) Clementz, M. A.; Chen, Z.; Banach, B. S.; Wang, Y.; Sun, L.; Ratia, K.; Baez-Santos, Y. M.; Wang, J.; Takayama, J.; Ghosh, A. K.; Li, K.; Mesecar, A. D.; Baker, S. C. Deubiquitinating and Interferon Antagonism Activities of Coronavirus Papain-like Proteases. *J. Virol.* **2010**, *84*, 4619−4629.
(29) Klemm, T.; Ebert, G.; Calleja, D. J.; Allison, C. C.; Richardson, L. W.; Bernardini, J. P.; Lu, B. G.; Kuchel, N. W.; Grohmann, C.; Shibata, Y.; Gan, Z. Y.; Cooney, J. P.; Doerflinger, M.; Au, A. E.; Blackmore, T. R.; van der Heden van Noort, G. J.; Geurink, P. P.; Ovaa, H.; Newman, J.; Riboldi-Tunnicliffe, A.; Czabotar, P. E.; Mitchell, J. P.; Feltham, R.; Lechtenberg, B. C.; Lowes, K. N.; Dewson, G.; Pellegrini, M.; Lessene, G.; Komander, D. Mechanism and Inhibition of The Papain-like Protease, PLpro, of SARS-CoV-2. *EMBO J.* **2020**, *39*, No. e106275.
(30) Pang, J.; Gao, S.; Sun, Z.; Yang, G. Discovery of Small Molecule PLpro Inhibitor Against COVID-19 Using Structure-Based Virtual Screening, Molecular Dynamics Simulation, and Molecular Mechanics/Generalized Born surface Area (MM/GBSA) Calculation. *Struct Chem* **2020**, *32*, 879.
(31) Xu, Y.; Chen, K.; Pan, J.; Lei, Y.; Zhang, D.; Fang, L.; Tang, J.; Chen, X.; Ma, Y.; Zheng, Y.; Zhang, B.; Zhou, Y.; Zhan, J.; Xu, W. Repurposing Clinically Approved Drugs for COVID-19 Treatment Targeting SARS-CoV-2 Papain-like Protease. *Int. J. Biol. Macromol.* **2021**, *188*, 137−146.
(32) Ma, L.; Wang, C.; He, Z.; Cheng, B.; Zheng, L.; Huang, K. Peptide-Drug Conjugate: A Novel Drug Design Approach. *Curr. Med. Chem.* **2017**, *24*, 3373−3396.
(33) Wang, Y.; Cheetham, A. G.; Angacian, G.; Su, H.; Xie, L.; Cui, H. Peptide-drug Conjugates as Effective Prodrug Strategies for Targeted Delivery. *Adv. Drug Delivery Rev.* **2017**, *110*−*111*, 112−126.
(34) Ratia, K.; Pegan, S.; Takayama, J.; Sleeman, K.; Coughlin, M.; Baliji, S.; Chaudhuri, R.; Fu, W.; Prabhakar, B. S.; Johnson, M. E.; Baker, S. C.; Ghosh, A. K.; Mesecar, A. D. A Noncovalent Class of Papain-like Protease/Deubiquitinase Inhibitors Blocks SARS Virus Replication. *Proc. Natl. Acad. Sci. U.S.A.* **2008**, *105*, 16119−16124.
(35) Wang, D.; Yu, M.; Liu, N.; Lian, C.; Hou, Z.; Wang, R.; Zhao, R.; Li, W.; Jiang, Y.; Shi, X.; Li, S.; Yin, F.; Li, Z. A Sulfonium Tethered Peptide Ligand Rapidly and Selectively Modifies Protein Cysteine in Vicinity. *Chem. Sci.* **2019**, *10*, 4966−4972.
(36) Liu, N.; Wang, D.; Lian, C.; Zhao, R.; Tu, L.; Zhang, Y.; Liu, J.; Zhu, H.; Yu, M.; Wan, C.; Li, D.; Li, S.; Yin, F.; Li, Z. Selective Covalent Targeting of Anti-apoptotic BFL-1 by a Sulfonium-Tethered Peptide. *Chembiochem* **2021**, *22*, 340−344.

https://doi.org/10.1021/acs.jmedchem.1c02022
J. Med. Chem. 2022, 65, 876−884